Chinese Medical Journal Pulmonary and Critical Care Medicine 3 (2025) 41–49

Contents lists available at ScienceDirect

Chinese Medical Journal Pulmonary and Critical Care Medicine

journal homepage: www.elsevier.com/locate/pccm

Original Article

Unraveling tumoral heterogeneity and angiogenesis-associated mechanisms of PD-1 and LAG-3 dual inhibition in lung cancers by single-cell RNA sequencing

Lishu Zhao[a,1], Chen Tang[b,1], Xuan Jin[b], Hao Wang[a], Kandi Xu[a], Xinyue Liu[a], Yujin Liu[a], Wencheng Zhao[a], Wengang Zhang[a], Li Ye[a], Zhimin Chen[a], Qi Liu[a,b,**], Yayi He[a,*]

[a] Department of Medical Oncology, Shanghai Pulmonary Hospital, Tongji University Medical School Cancer Institute, School of Medicine, Tongji University, Shanghai 200433, China

[b] Key Laboratory of Spine and Spinal Cord Injury Repair and Regeneration (Tongji University), Ministry of Education, Orthopedic Department of Tongji Hospital, Frontier Science Center for Stem Cell Research, Bioinformatics Department, School of Life Sciences and Technology, Tongji University, Shanghai 200092, China

ARTICLE INFO

Edited by: Peifang Wei

Keywords:
Lung cancer
Immunotherapy
Programmed death 1 (PD-1)
Lymphocyte activation gene 3 (LAG-3)
Tumor heterogeneity
Tumor angiogenesis

ABSTRACT

Background: Lymphocyte activation gene 3 (LAG-3) is a promising immune checkpoint for combination immunotherapy. This study aims to elucidate the exact synergistic anti-tumor mechanism of programmed death 1 (PD-1) and LAG-3 dual inhibition in lung cancer.

Methods: Multiple patient-derived xenograft (PDX) models of lung cancer were constructed and analyzed by single-cell RNA sequencing (scRNA-seq). Clustering of all human-derived cells, identification of biomarker genes of three cell types, trajectory analysis, and calculation of tumor heterogeneity scores were performed. Differentially expressed genes (DEGs) were identified and functional enrichment analyses of cancer-associated genes were conducted. The functional significance of DEGs in the immune system was evaluated using the Reactome online server. Major histocompatibility complex (MHC) pathways and angiogenesis-associated pathways were analyzed. The Cancer Genome Atlas (TCGA) was used for further verification.

Results: PD-1 and LAG-3 dual inhibition achieved synergistic tumor inhibition in squamous cell carcinoma (SCC) PDX models, but not in adenocarcinoma and small cell lung cancer PDX models. A total of 8127 cells, including 2699 basal, 4109 malignant, and 1319 epithelial cells, were identified by scRNA-seq. Malignant cells evolved from basal and epithelial cells in the trajectory analysis. The responders to the combination therapy of PD-1 and LAG-3 inhibitors had lower heterogeneity scores than non-responders. Compared with anti-PD-1 monotherapy, the combination group exhibited higher levels of neutrophil degranulation. The DEGs were correlated with disease, metabolism, and programmed cell death-associated pathways. The MHC class I-associated pathways and pericyte pathways were upregulated, whereas the vascular endothelial growth factor pathway was downregulated in the combination group.

Conclusion: We discovered the superior efficacy of PD-1 and LAG-3 dual inhibition in SCC PDX models, and showed that it may be associated with low tumor heterogeneity scores, upregulation of the MHC class I pathway, and normalization of tumor angiogenesis.

Introduction

Lung cancers can be classified as small cell lung cancer (SCLC) and non-small-cell lung cancer (NSCLC), and are the main contributors to cancer-related mortality worldwide.[1,2] Immunotherapy using programmed death 1 (PD-1) and programmed death-ligand 1 (PD-L1) inhibitors has significantly improved the outcomes of patients with SCLC or NSCLC.[3,4] However, most patients with lung cancer fail to respond to single immunotherapy due to primary or secondary resistance. Multiple strategies have been devised to address these resistances and promote more durable responses. Combination therapy based on PD-1/PD-L1 inhibitors has been extensively explored to enhance the

* Corresponding author at: Department of Medical Oncology, Shanghai Pulmonary Hospital, School of Medicine, Tongji University, Shanghai 200433, China
** Corresponding author at: Key Laboratory of Spine and Spinal Cord Injury Repair and Regeneration (Tongji University), Ministry of Education, Orthopaedic Department of Tongji Hospital, Frontier Science Center for Stem Cell Research, Bioinformatics Department, School of Life Sciences and Technology, Tongji University, Shanghai 200092, China
E-mail addresses: yayi.he@tongji.edu.cn (Y. He), qiliu@tongji.edu.cn (Q. Liu)
[1] Lishu Zhao and Chen Tang contributed equally to this work.

https://doi.org/10.1016/j.pccm.2025.02.004
Received 26 June 2024; Available online 14 March 2025

response, including immunotherapy and chemotherapy.[5] Selecting the appropriate combination strategy can greatly improve the prognosis of patients with lung cancers.

Co-expression of multiple immune checkpoints is a common phenomenon in many solid cancers[6] and hematologic tumors,[7] which provides an opportunity for immunotherapy combination regimens. In a previous study,[8] we detected a high level of co-expression of lymphocyte activation gene 3 (LAG-3) and PD-1/PD-L1 in the immune checkpoint landscape of NSCLC. We also demonstrated that LAG-3 was associated with PD-1/PD-L1 in patients with SCLC.[9] LAG-3 was also found to be both an efficacy predictor and prognostic factor of NSCLC.[10,11] For instance, increased LAG-3 expression was associated with a lower objective response rate and shorter progression-free survival among patients with NSCLC receiving PD-1 inhibitors.[11] These results suggest that LAG-3 may be a promising target for treating NSCLC.

Preliminary studies have shown that blocking LAG-3 reduced immunosuppressive cytokine secretion and reinvigorated exhausted $CD4^+$ and $CD8^+$ T cells.[12,13] Simultaneously targeting PD-1 and LAG-3 has demonstrated promising anti-cancer efficacy in clinical trials for multiple solid tumors such as NSCLC[14] and melanoma.[15] A phase 3 clinical trial showed that patients with melanoma who were treated with PD-1 and LAG-3 dual blockades had a higher objective response rate and significantly superior progression-free survival than patients with melanoma who received PD-1 inhibitors.[15] However, the synergistic effect of this combination therapy and its potential molecular mechanisms remain to be fully elucidated in lung cancer.

Here, we aimed to assess the synergistic effectiveness of PD-1 and LAG-3 dual inhibitors among patient-derived xenograft (PDX) models constructed from tumor specimens from lung cancer patients and peripheral blood mononuclear cells (PBMCs) from the same patients. Subsequently, single-cell RNA sequencing (scRNA-seq) and bioinformatic analyses were performed to elucidate the underlying mechanisms by which PD-1 and LAG-3 inhibitors exerted their effects.

Methods

Study design, patient tumor specimen processing, and isolation of PBMCs

Five types of PDX models were constructed from five patients, including two with squamous cell carcinoma (SCC) (patient No. 1038 and No. 1144), two with adenocarcinoma (ADC) (patient No. 1131 and No. 1078), and one with SCLC (patient No. 1180). Lung cancer tissues were collected by computed tomography-guided percutaneous puncture biopsy of lung or lymph nodes, and PBMCs were isolated from venous blood at Shanghai Pulmonary Hospital between January 1, 2019 and December 31, 2020. The study was approved by the Ethics Committee of Shanghai Pulmonary Hospital (No. K22-241) and conformed to the principles of the *Declaration of Helsinki* and its later amendments. All patients signed written informed consent.

PDX model construction and immunotherapy application

Female NOD/Shi-scid/IL-2Rγ^{null} (NOG) mice, provided by Charles River (Beijing) in China, were used to construct the PDX models. All animal care, treatment, welfare, and sacrifice procedures abided by the regulations of the Ethics Committee of Shanghai Pulmonary Hospital (No. K22-241). The detailed procedures of PDX establishment and tumor passage were as described previously.[16] PBMCs from the same patient were intravenously injected into the NOG mice to rebuild their immune system. Mouse weight and tumor volume were measured twice a week to generate tumor growth curves. All the PDX models from the same patient were randomly divided into four treatment groups: PD-1 inhibitors, LAG-3 inhibitors, PD-1 + LAG-3 inhibitors, and placebo. Immunotherapy was initiated when the tumors grew to approximately 100 mm^3 (Fig. 1A). The dosing regimen for both the PD-1 and LAG-3 inhibitors in the PDX models was 10 mg/kg, which was administered intraperitoneally in a single dose. After 3 weeks of monitoring the tumor size, the mice were euthanized to collect and sequence the tumors.

Single-cell preparation and scRNA-seq

Tumor specimens were digested in 2 mL of tissue dissociation solution at 37°C for 15 min to obtain a single-cell suspension. Single-cell samples were sequenced on a 10 × Genomics platform (Singleron Biotechnologies, Suzhou, Jiangsu, China). The detailed procedures for RNA extraction and scRNA-seq library preparation were as described previously.[17,18]

Quality control, dimensionality reduction, clustering, and annotation

The scRNA-seq data were pre-processed using the Cell Ranger toolkit (version 3.1.0, Singleron Biotechnologies) provided by 10 × Genomics. The toolkit was used to aggregate raw data, filter out low-quality reads, align reads to the Genome Research Consortium human 38 (GRCh38) human reference genome, assign cell barcodes, and construct a unique molecular identifier (UMI) matrix. Seurat (https://satijalab.org/seurat/) was used for the subsequent scRNA-seq data analyses. Specifically, the raw UMI matrix was processed to remove low-quality cells; namely, cells with <200 detected genes or >5 % mitochondrial gene content. The aim of this filtering process was to preserve major heterogeneous cell types for subsequent analysis.

After the low-quality cells were removed, the raw UMI matrices (representing gene expression matrices) were normalized to account for the total cellular and mitochondrial read counts, and the original sample identities. Normalization was carried out using linear regression and the Regress Out function in Seurat (https://satijalab.org/seurat/). Dimensionality reduction techniques were used to summarize the variably expressed genes. Principal component analyses were performed to summarize the genes using the first 100 principal components. Subsequently, the Uniform Manifold Approximation and Projection (UMAP) dimensionality reduction technique was used with default settings in the RunUMAP function to further summarize the components. For clustering, we used the FindClusters function with 50 principal components, which assigned the cells into distinct clusters based on their similarity. To identify the biological cell types in the clusters, we annotated them using canonical marker genes. The FindAllMarkers function in Seurat was used to identify marker genes that were enriched in each cluster and to compare the gene expression profiles of cells in a specific cluster with those in all the other clusters.

To qualify as marker genes, their average expression in a specific cluster had to be >2.5 times higher than their expression in all the other clusters. The marker genes were used to annotate cell types by comparing them with the gene signature obtained from the CellMarker database, which includes basal cells (CDC28 protein kinase regulatory subunit 2 [*CKS2*], targeting protein for xenopus kinesin-like protein 2 [*TPX2*], centromere protein F 21 [*CENPF21*]), epithelial cells (glycoprotein non-metastatic melanoma protein B [*GPNMB*], aldo-keto reductase family 1 member C1 [*AKR1C1*], lymphocyte antigen 6 family member D [*LY6D*]), and malignant cells (S100 calcium binding protein A7 like 2 [*S100A7L2*], carnosine dipeptidase 2 [*CN2/CNDP2*], cornifelin [*CNFN*]).

To distinguish malignant and non-malignant cells, two criteria were applied: (1) analysis of inferred copy number variation (CNV) profiles, and (2) under-expression patterns typical of different non-malignant cell types. We used CopyKAT (https://github.com/navinlabcode/copykat) to accurately detect cancerous cells by calculating the CNV for each individual cell.

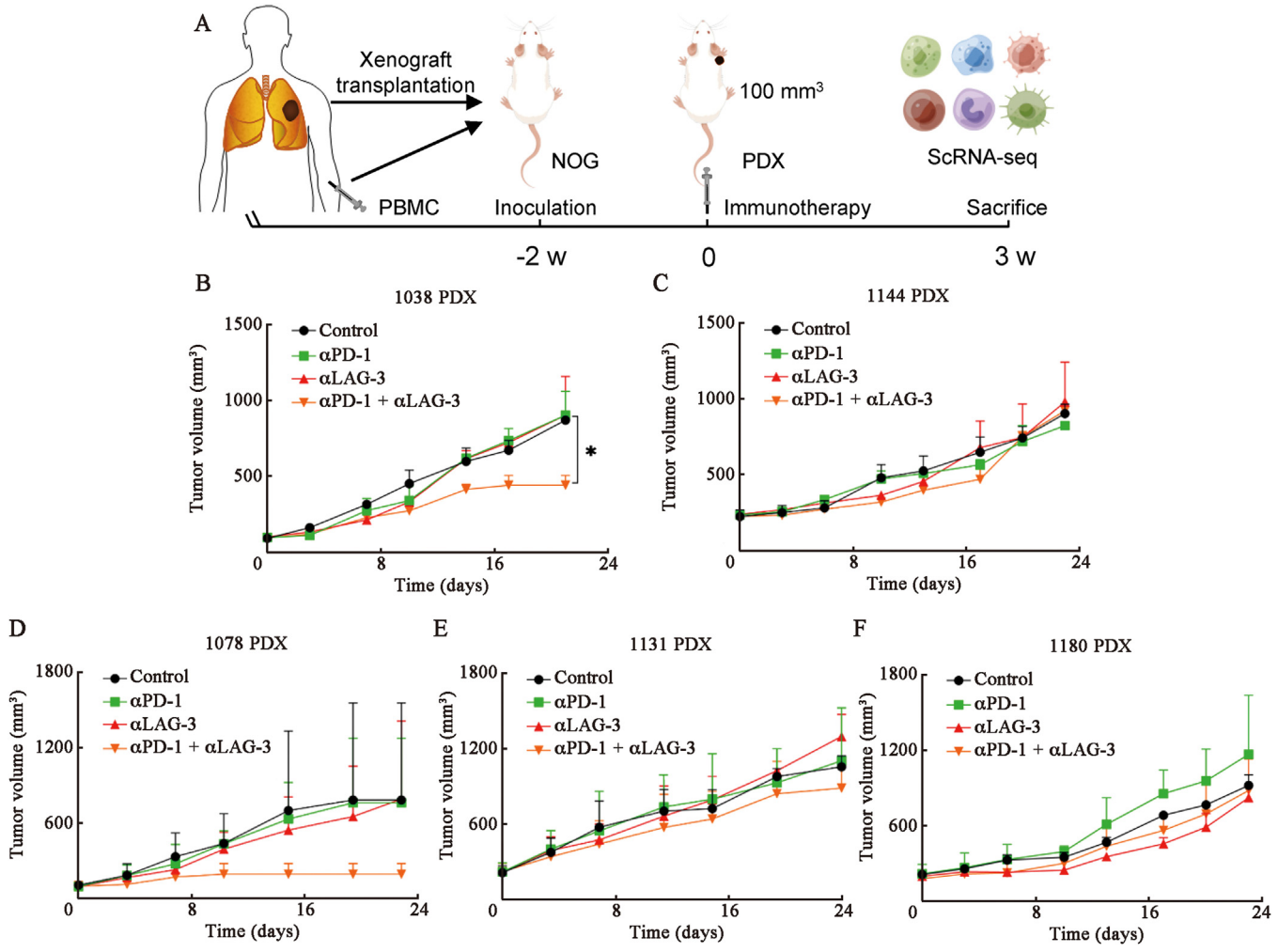

Fig. 1. Antitumor efficacy of PD-1 and LAG-3 inhibitors in multiple PDX models. (A) Research design and treatment timeline. Tumor growth curves of PDX models constructed from patients No. 1038 (B), 1144 (C), 1078 (D), 1131 (E), and 1180 (F) who received intraperitoneal injection of either vehicle, αLAG-3, αPD-1, or a combination of both. $^{*}P$ <0.05 for comparison between αPD-1 and combination therapy group. αLAG-3: Anti-LAG-3 antibody; αPD-1: Anti-PD-1 antibody; LAG-3: Lymphocyte activation gene 3; NOG: *NOD/Shi-scid/IL-2Rγ*^{null}; PBMC: Peripheral blood mononuclear cells; PD-1: Programmed death 1; PDX: Patient-derived xenograft; ScRNA-seq: Single-cell RNA sequencing; w: Week.

Differentially expressed genes (DEGs) and enrichment analysis

The Wilcoxon tests in the FindMarkers function were used to identify DEGs across different treatment conditions and cell types. The enrichGO function in the clusterProfiler package in R (https://www.bioconductor.org/packages/devel/bioc/html/clusterProfiler.html) was used for functional enrichment analyses of the DEGs. Unexpected functional relationships between DEGs were further analyzed using the Reactome Knowledgebase, which provides detailed information on signal transduction, transport, DNA replication, and metabolism.

Developmental trajectory analysis

To generate a developmental trajectory, we performed pseudotime analysis of different cell types using the Monocle (version 3) algorithm with the gene expression matrix derived from the Seurat subset as input. To create an object, we used the Cell Data Set function with the expressionFamily parameter set to negative binomial to accommodate the nature of our expression data. Following dimensionality reduction and cell sorting, default parameters were used to infer the cell trajectory.

Analysis of external lung cancer data from The Cancer Genome Atlas (TCGA)

Transcriptomic information from two NSCLC cohorts was extracted from TCGA data collection (https://portal.gdc.cancer.gov/projects/TCGA-LUAD; https://portal.gdc.cancer.gov/projects/TCGA-LUSC) to verify differences in LAG-3 levels between patients with SCC and patients with ADC, as well as the associations of LAG-3 levels with the degree of enrichment in pericyte pathways.

Statistical analysis

Tumor growth curves were compared by two-way repeated measures analysis of variance (ANOVA) with GraphPad Prism 8 (GraphPad Software, La Jolla, CA, USA). For comparisons where the initial *P* values were less than 0.05, multiple pairwise comparisons were conducted using Tukey's tests to assess the difference in the effects of different therapies. To analyze survival data, we used various functions from the survival package in R (https://www.r-project.org/); namely, log-rank tests to compare survival distributions. To further validate the relationship between the enriched pathways and survival outcomes, patients were divided into two groups (high *vs.* low) based on the median level of

pathway activation. *P*-values <0.05 were considered statistically significant.

Results

Construction of PDX models of lung cancer and the synergistic effects of PD-1 and LAG-3 dual blockade in PDX models

We constructed five types of PDX models from five lung cancer patients; two with SCC (patient No. 1038 and No. 1144), one with ADC with an *EGFR* L858R mutation (patient No. 1131), one with wild-type ADC (patient No. 1078), and one with SCLC (patient No. 1180). The clinicopathological information for these patients is listed in Supplementary Table 1. By comparing the tumor growth curves of the four treatment groups (PD-1 inhibitors *vs.* LAG-3 inhibitors *vs.* LAG-3 + PD-1 inhibitors *vs.* placebo) of PDX models, we found that PD-1 and LAG-3 dual blockades had significant synergistic antitumor effects on No. 1038 SCC PDX (PD-1 inhibitors *vs.* PD-1 + LAG-3 inhibitors; $P = 0.024$; Fig. 1B) but not on No. 1144 SCC PDX, ADC PDX, and SCLC PDX models (all $P > 0.05$; Fig. 1C–F).

Single-cell landscape of PDX tumor models

One tumor from each treatment group of the SCC PDX models (No. 1038: Animal No. 756, 776, 751, and 763; No. 1144: Animal No. 976, 977, 980, and 992) was selected and prepared for single-cell sequencing. After excluding mouse cells, a total of 8127 human-derived cells remained for further analysis. Clustering analyses of all cells from No. 1038 SCC PDX (Fig. 2A) and No. 1144 SCC PDX (Fig. 2B) models were performed. Three clusters were identified by UMAP visualization; namely, 2699 basal, 1319 epithelial, and 4109 malignant cells. The top 10 DEGs in the three cell types are shown in Fig. 2C.

We identified representative biomarker genes for PD-1 and LAG-3 dual inhibitor responder No. 1038 (Fig. 2D). Single-cell trajectory analysis of No. 1038 showed that malignant cells evolved from both basal and epithelial cells (Fig. 2E). The CNV profiles of malignant cells (Fig. 2F) indicated that they could be divided into nine subclusters (Fig. 2G). The tumor heterogeneity score of the responders was lower than that of the non-responders (Figs. 2H, I).

DEGs between the PD-1 and LAG-3 inhibitor combination therapy group and PD-1 monotherapy group

Because we observed a synergistic effect of PD-1 and LAG-3 dual inhibitors on the No. 1038 PDX models, we analyzed the DEGs between PD-1 and LAG-3 dual inhibition and PD-1 monotherapy. A total of 83 cancer-associated genes were differentially expressed in the malignant cells. A volcano plot showed that mitochondrially encoded NADH: ubiquinone oxidoreductase core subunit 4 L (*MT-ND4 L*) and mitochondrially encoded ATP synthase 6 pseudogene 1 (*MTATP6P*1) were significantly upregulated, and thymosin beta 4 X-linked (*TMSB4X*), collagen type I alpha 2 chain (*COL1A2*), and interferon alpha inducible protein 27 (*IFI27*) were downregulated (Fig. 3A). The gene ontology (GO) enrichment analysis showed that the DEGs may be involved in multiple pathways, including translational initiation, protein localization to endoplasmic reticulum, ribosome, and structural constituent of ribosome pathways (Fig. 3B).

The GO enrichment analyses of all the DEGs showed that they were enriched in multiple pathways, including neutrophil degranulation, anchoring fibril formation, MET activating PTK2 protein tyrosine kinase 2 (PTK2) signaling, and IL-4/IL-13 signaling (Supplementary Table 2). Using TCGA public data, we verified that patients with high neutrophil degranulation (*P*-value = 0.011, Fig. 3C) had statistically poorer survival outcomes.

The functional significance of DEGs in the immune system was further verified using the Reactome online server. We found that pathways associated with disease, metabolism, and programmed cell death were marked with dark yellow, indicating a close correlation between DEGs and these pathways (Fig. 4).

Upregulation of the major histocompatibility complex class I (MHC class I) pathway in PD-1 and LAG-3 dual inhibitor responders

MHC class I-associated pathways, including MHC class I-mediated antigen processing and presentation, as well as antigen presentation: folding, assembly, and peptide loading of MHC class I, were significantly enriched in PDX models receiving PD-1 and LAG-3 dual inhibitors compared with their levels in PDX models receiving PD-1 monotherapy (Table 1). These findings suggest that the MHC class I pathway may be significantly involved in the synergistic anti-tumor effects of combined PD-1 and LAG-3 immunotherapy.

PD-1 and LAG-3 dual inhibitors promote the normalization of tumor angiogenesis

By analyzing angiogenesis-associated genes and cells, we found that pericyte pathways were notably more activated in the group treated with PD-1 and LAG-3 dual inhibitors than they were in the PD-1 monotherapy group (Fig. 5A). Compared with the results of the PD-1 monotherapy, the combination therapy led to significant downregulation of multiple pathways, including the Janus kinase/signal transducer and activator of transcription (JAK/STAT) pathway and vascular endothelial growth factor (VEGF) pathway (Fig. 5B). These findings suggest that PD-1 with LAG-3 dual inhibitors may contribute to tumor vessel normalization. We also found that the expression level of LAG-3 was higher in SCC than it was in TCGA-LUAD public data (Fig. 5C), and LAG-3 was significantly associated with pericyte pathways in SCC but not in ADC (Figs. 5D, E). These findings partly explain the superior efficacy of combination immunotherapy in patients with SCC compared with its efficacy in patients with ADC.

Discussion

The combination therapy strategy of PD-1 and LAG-3 dual inhibitors demonstrated a higher level of effectiveness compared with PD-1/PD-L1 blockade alone. However, the precise underlying mechanisms warrant further investigation. In the present study, we developed multiple PDX models and showed that PD-1 and LAG-3 dual inhibitors had greater efficacy than PD-1 monotherapy in the No. 1038 SCC PDX model. The scRNA-seq analysis showed that the synergistic effects of PD-1 and LAG-3 dual inhibition may be associated with a lower degree of tumor heterogeneity, upregulation of the MHC class I pathway, and normalization of tumor angiogenesis. Elucidating these mechanisms may offer insights into more effective cancer immunotherapies.

We found a synergistic anti-tumor effect of combination immunotherapy in a SCC PDX model but not in ADC or SCLC PDX models. Similar results were observed in other SCCs, such as head and neck SCC.[14] In a previous study, we demonstrated that LAG-3 levels on tumor-infiltrating cells in non-ADC (82 % were SCC) were prominently higher than those in ADC.[10] Multiple studies have shown that LAG-3 is an efficacy predictive biomarker of PD-1 inhibitors in NSCLC,[11] hepatocellular carcinoma,[19] gastric cancer,[20] and other cancers. Combining LAG-3 with PD-1 inhibitors was associated with longer progression-free survival in patients with melanoma with LAG-3 expression ≥1 %.[21] These findings indicate that the high expression levels of LAG-3 in the SCC PDX model may partly contribute to the superior efficacy of the combination immunotherapy. Detection of LAG-3 expression in the tumor microenvironment may help to predict whether patients

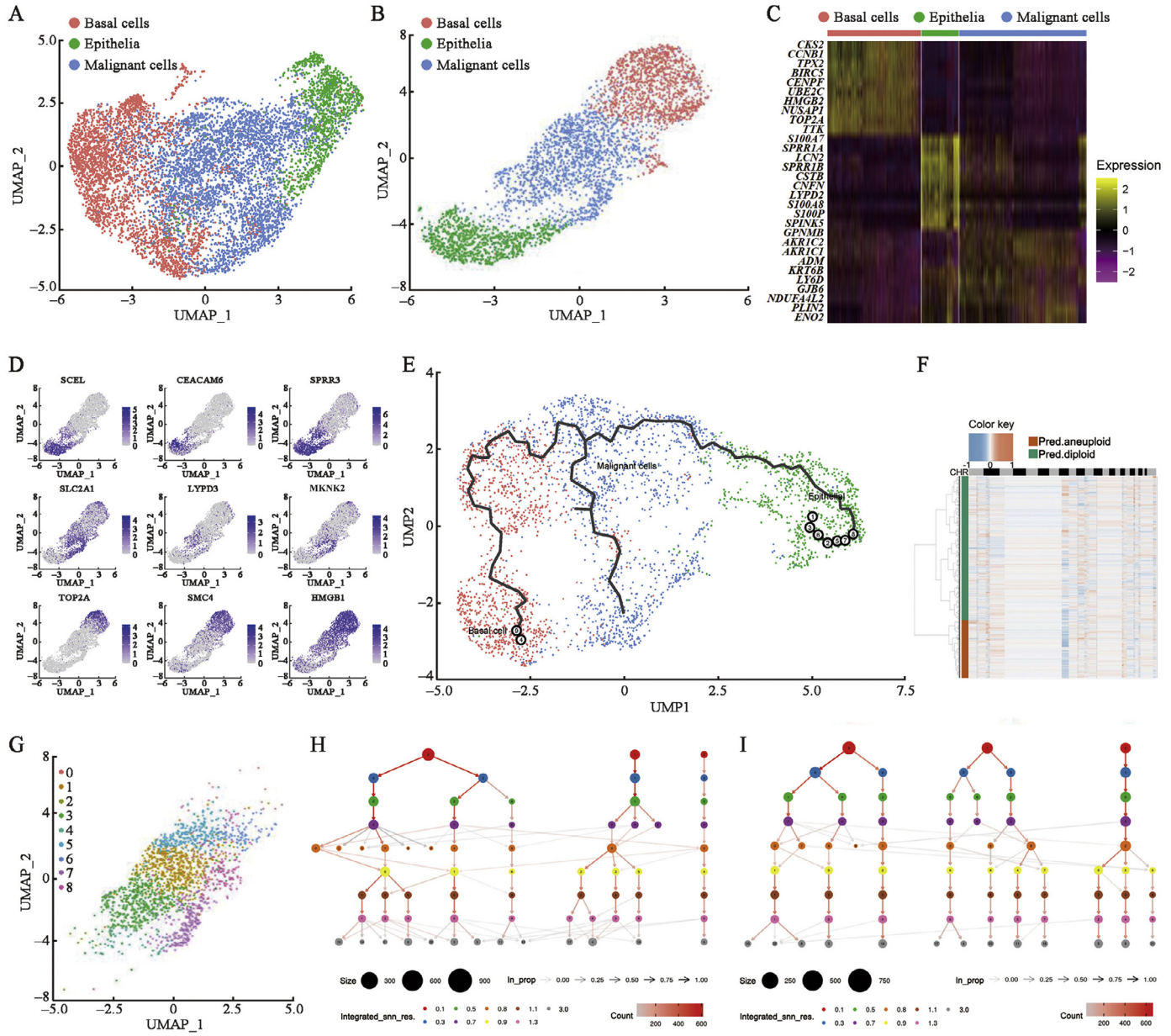

Fig. 2. Single-cell landscape of tumor tissues in SCC PDX models. UMAP visualization of all cell clusters from No. 1038 SCC PDX (A) and No.1144 SCC PDX (B) models; top 10 DEGs of three cell types (C); representative biomarker genes (D); single-cell trajectory analysis (E), CNV of malignant cells (F), and nine subclusters of malignant cells (G) of No. 1038 SCC PDXs; tumor heterogeneity scores of responders (H) and non-responders (I). The numbered cells in (E) represent the cells with the lowest pseudotime values, indicating the initial state cells. *ADM*: Adrenomedullin; *AKR1C1*: Aldo-keto reductase family 1 member C1; *AKR1C2*: Aldo-keto reductase family 1 member C2; *BIRC5*: Baculoviral inhibitor of apoptosis repeat containing 5; *CCNB1*: Cyclin B1; *CENPF*: Centromere protein F; CHR: Chromosome; *CKS2*: CDC28 protein kinase regulatory subunit 2; *CEACAM6:* Carcinoembryonic antigen-related cell adhesion molecule 6; *CNFN*: Cornifelin; CNV: Copy number variation; *CSTB*: Cathepsin B; DEGs: Differentially expressed genes; *ENO2*: Enolase 2; *GJB6*: Gap junction protein beta 6; *GPNMB*: Glycoprotein non-metastatic melanoma protein B; *HMGB1*: High-mobility group box 1; *HMGB2*: High-mobility group box 2; *KRT6B*: Keratin 6B; *LCN2*: Lipocalin 2; *LYPD2*: LY6/PLAUR domain containing 2; LYPD3: LY6/PLAUR domain containing 3; *LY6D*: Lymphocyte antigen 6 family member D; *MKNK2*: MAPK interacting serine/threonine kinase 2; *NDUFA4L2*: NADH dehydrogenase (ubiquinone) 1 alpha subcomplex, 4-like 2; *NUSAP1*: Nucleolar and spindle-associated protein 1; PDX: Patient-derived xenograft; *PLIN2*: Perilipin 2; *S100A7*: S100 calcium binding protein A7; *S100A8*: S100 calcium binding protein A8; *S100P*: S100 calcium binding protein; SCC: Squamous cell carcinoma; *SCEL:* Sciellin; *SLC2A1*: Solute carrier family 2 member 1; *SMC4*: Smc4-structural maintenance of chromosomes 4; *SPINK5*: Serine peptidase inhibitor Kazal type 5; *SPRR3:* Small proline rich protein *3*; *SPRR1A*: Small proline rich protein 1A; *SPRR1B*: Small proline rich protein 1B; *TPX2*: Targeting protein for xenopus kinesin-like protein 2; *TOP2A*: Topoisomerase IIα; *TTK*: Threonine tyrosine kinase; *UBE2C*: Ubiquitin-conjugating enzyme 2C; UMAP: Uniform manifold approximation and projection.

would benefit from LAG-3 inhibitors and dynamic monitoring of LAG-3 may help determine the appropriate intervention timing for LAG-3 inhibitors.

We also found that the SCC PDX model that was responsive to PD-1 and LAG-3 dual inhibitors had a low degree of tumor heterogeneity. Intratumoral heterogeneity is a negative predictive biomarker for multiple immunotherapy regimens in various solid tumors, including NSCLC. For instance, Fang *et al*[22] demonstrated that patients with NSCLC with low tumor heterogeneity had a high objective response rate and durable clinical benefit. Therefore, the synergistic anti-tumor effects of PD-1 and

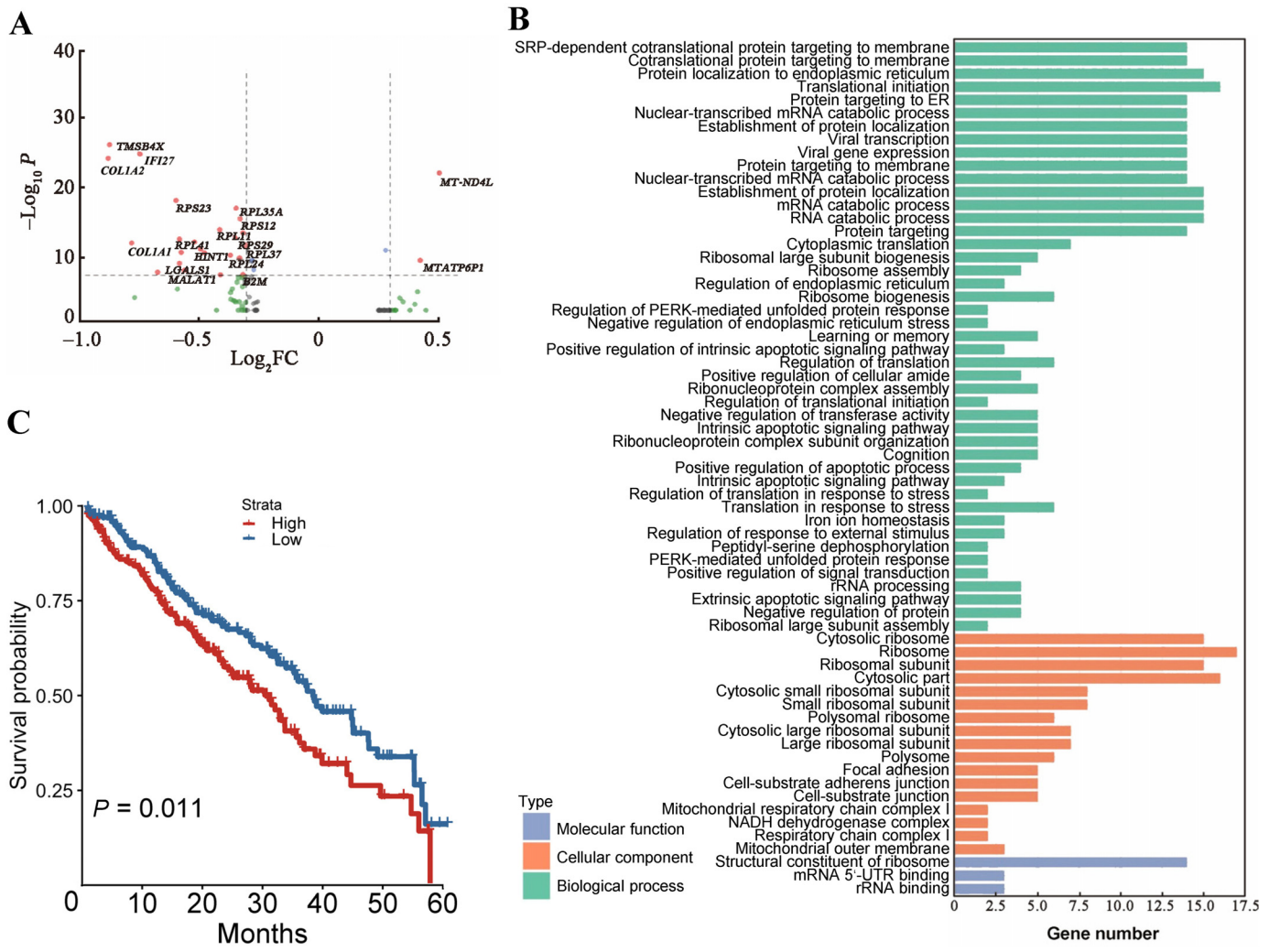

Fig. 3. DEGs and enrichment analyses. Volcano plot (A) and GO enrichment analyses (B) of differentially expressed cancer-associated genes between the combination group and PD-1 monotherapy group among No. 1038 SCC PDX model; (C) association of neutrophil degranulation with survival outcome in TCGA-LUSC public data with patients divided into two groups (high *vs.* low) based on the median level of pathway activation. In figure (A), gray dots mean genes with no significant differential expression, green dots mean genes with significant differential expression based on fold change (|fold change| ≥1.2), blue dots mean genes with significant differential expression based on *P* values $<10^{-7}$, and red dots mean genes with significant differential expression based on fold change (|fold change| ≥1.2) and *P* values $<10^{-7}$. B2M: Beta-2-microglobulin; *COL1A1*: Collagen type I alpha 1 chain; *COL1A2*: Collagen type I alpha 2 chain; DEGs: Differentially expressed genes; ER: Endoplasmic reticulum; FC: Fold change; GO: Gene ontology; *HINT1*: Histidine triad nucleotide binding protein 1; *IFI27*: Interferon alpha inducible protein 27; *LGALS1*: Lecticin, galactoside-binding, soluble 1; LUAD: Lung adenocarcinoma; *MALAT1*: Metastasis associated lung adenocarcinoma transcript 1; mRNA: Messenger RNA; *MTATP6P1*: Mitochondrially encoded ATP synthase 6 pseudogene 1; *MT-ND4L*: Mitochondrially encoded NADH: ubiquinone oxidoreductase core subunit 4 L; NADH: Nicotinamide adenine dinucleotide; PD-1: Programmed death 1; PDX: Patient-derived xenograft; PERK: Protein kinase R-like endoplasmic reticulum kinase; *RPL11*: Ribosomal protein L11; *RPL24*: Ribosomal protein L24; *RPL35A*: Ribosomal protein L35a; *RPL37*: Ribosomal protein L37; *RPL41*: Ribosomal protein L41; *RPS12*: Ribosomal protein S12; *RPS23*: Ribosomal protein S23; *RPS29*: Ribosomal protein S29; rRNA: Ribosomal RNA; SCC: Squamous cell carcinoma; SRP: Signal recognition particle; TCGA: The Cancer Genome Atlas; *TMSB4X*: Thymosin beta 4 X-linked; UTR: Untranslated region.

LAG-3 dual inhibition may be partly attributed to decreased tumor heterogeneity.

The MHC class I pathway was also involved in the anti-tumor effects of combining PD-1 and LAG-3 inhibitors. LAG-3 has several ligands, such as fibrinogen-like protein 1 and galectin-3, with MHC class II being the most canonical ligand.[12] LAG-3 binding to its ligands inhibits inflammatory cytokine secretion and immune cell activation, including CD4/$CD8^+$ tumor-infiltrating cells and dendritic cells.[23-25] Unexpectedly, we found that the MHC class I pathway was upregulated after treatment with PD-1 and LAG-3 dual inhibitors. LAG-3 is preferentially expressed on activated $CD8^+$ T cells, and CD8 specifically recognizes MHC class I molecules.[26] Previous studies using immunofluorescence microscopy to detect the co-localization of LAG-3 and MHC class I have proven that there is a presence of LAG-3 co-caps on cells that are capped with MHC class I molecules.[27] Additionally, LAG-3 was reported to be positively co-expressed with genes associated with both MHC calss I and MHC calss II across multiple cancers.[28] Together, these findings suggest that MHC class I may be involved in the anti-cancer properties of LAG-3 inhibitors, but the detailed mechanisms remain to be elucidated.

The pericyte pathway was upregulated and the VEGF pathway was downregulated in the combination group in our study. Pericytes, also called mural cells, are located in the basement membrane of vessels and are closely correlated with endothelial cells to sustain the function

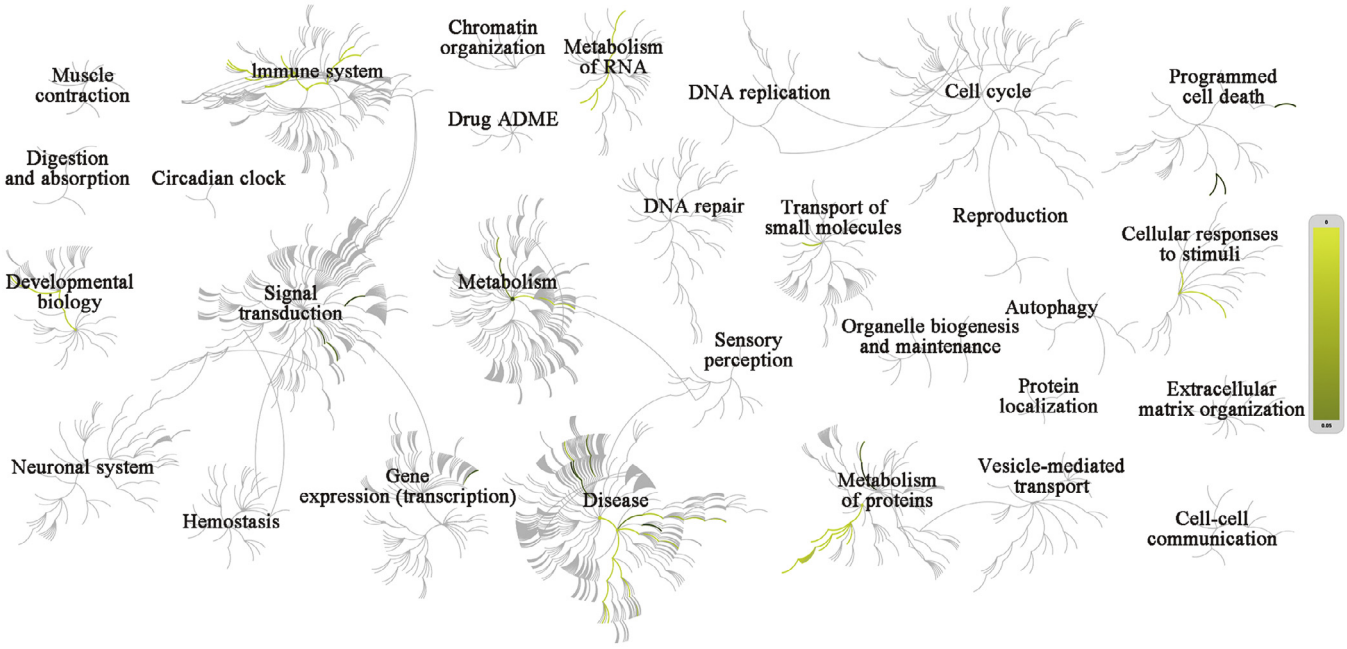

Fig. 4. Functional significance of DEGs in the immune system portrayed on the Reactome online server. ADME: Absorption, distribution, metabolism, excretion; DEGs: Differentially expressed genes.

Table 1
Upregulation of MHC class I-associated pathways in the SCC PDX responder of PD-1 and LAG-3 dual inhibition.

Pathway name	Entities found*	Ratio	*P*-value	FDR	Reactions found†	Ratio
Immunoregulatory interactions between a lymphoid and a non-lymphoid cell	22/316	0.021	<0.001	<0.001	13/44	0.003
Selenocysteine synthesis	18/112	0.007	<0.001	<0.001	2/7	<0.001
Antigen presentation: folding, assembly and peptide loading of class I MHC	22/108	0.007	<0.001	<0.001	13/16	0.001
Class I MHC-mediated antigen processing and presentation	24/479	0.032	<0.001	<0.001	24/48	0.003

* The numbers in this column represent the number of input genes overlapping with a given pathway (numerator), relative to the total number of annotated genes in that pathway (denominator).
† The numbers in this column represent the number of biochemical reactions or molecular interactions linked to the identified entities (e.g., proteins, genes), compared to the total number of entities within a given pathway. FDR: False discovery rate; LAG-3: Lymphocyte activation gene 3; MHC: Major histocompatibility complex; PD-1: Programmed death 1; PDX: Patient-derived xenograft; SCC: Squamous cell carcinoma.

of the vasculature.[29] However, the vessels of tumors are leaky because pericyte coverage is defective, and the interaction between pericytes and endothelial cells is impaired, which affects the permeation of antitumor drugs.[29] VEGF drives abnormal angiogenesis in tumors,[30] and high VEGF levels have been shown to predict poorer survival outcomes in multiple cancers, including NSCLC[31] and hepatic cancer.[32] In our study, PD-1 and LAG-3 dual inhibition increased the recruitment of pericytes and downregulated the expression of VEGF. These results indicate that LAG-3 inhibitors may function partially by promoting the normalization of tumor vessels, thereby augmenting the delivery of anti-tumor drugs.

Increased neutrophil degranulation was observed in responders to PD-1 and LAG-3 dual inhibitors. Neutrophil degranulation is the migration of neutrophil cytoplasmic granules to merge with the cell or phagosome membrane, leading to granule exocytosis or release on the cell surface.[33] Neutrophil degranulation on the one hand can facilitate the transportation of tumor cells and promote tumor progression,[33] on the other hand, regulate adaptive immunity by enhancing the activation and tumor infiltration of T lymphocytes.[34,35] Previous studies have noted that immunotherapy alters the status of neutrophil degranulation.[34,36,37] For instance, proteomic analysis showed that anti-PD-1 therapy induced neutrophil degranulation in pancreatic ADC[34] and metastatic cutaneous melanoma.[37] However, Kaisar-Iluz *et al*[36] reported that PD-L1 inhibitors decreased neutrophil degranulation in lung cancer models. These seemingly contradictory findings suggest that the immune modulatory effect of neutrophil degranulation may vary among different cancer types.

This study has several limitations. First, the number of PDX models used in the study was limited, necessitating further comprehensive investigations in future studies. Second, the number of immune cells in the PDX models was limited and reduced during tumor progression. This limitation hinders the understanding of the tumor immune microenvironment posttreatment, complicating the investigation of immune-mediated antitumor mechanisms in the combination immunotherapy.

In conclusion, our findings provide evidence of a synergistic antitumor effect resulting from PD-1 and LAG-3 dual inhibitors in an SCC PDX model. We also found that this effect may be correlated with a low tumor heterogeneity score, upregulation of the MHC class I pathway, and normalization of tumor angiogenesis by scRNA-seq analyses. These important discoveries hold promise for refining the approach to selecting patients who may benefit from combined immunotherapy.

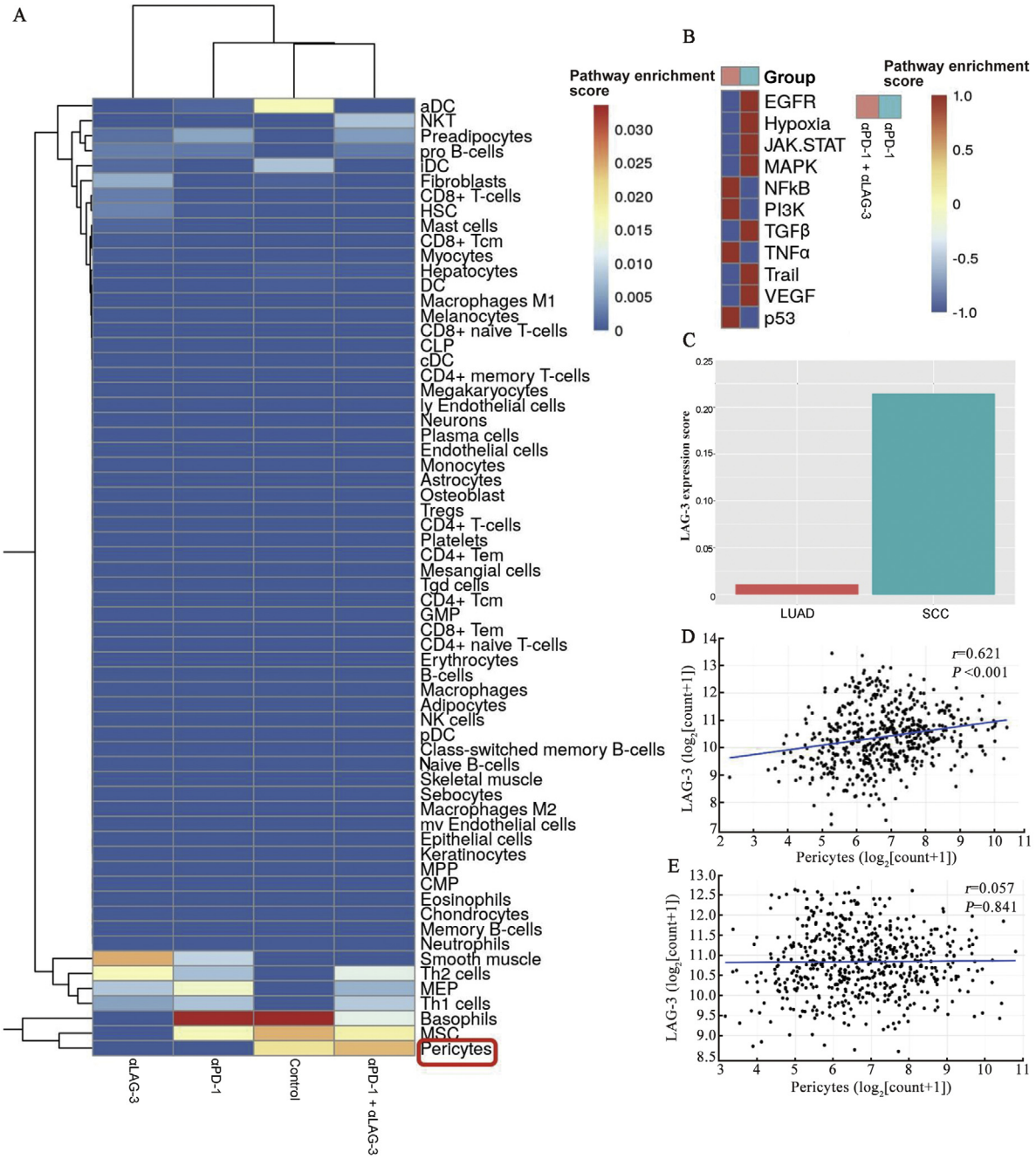

Fig. 5. Combining PD-1 and LAG-3 inhibitors promotes the normalization of tumor angiogenesis. Angiogenesis-associated pathways were compared among the PD-1 and LAG-3 dual inhibition and monotherapy treatment groups (A); expression of multiple pathways, including the JAK/STAT pathway and VEGF pathway, which was significantly downregulated in the combination group versus the PD-1 inhibitor group (B); expression level of LAG-3 between SCC and ADC in TCGA-LUAD public data (C); association of LAG-3 expression with pericyte pathway expression in SCC ($n = 630$) and ADC ($n = 706$) (D, E). αLAG-3: Anti-LAG-3 antibody; αPD-1: Anti-PD-1 antibody; aDC: Activated dentritic cell; ADC: Adenocarcinoma; CLP: Common lymphoid precursor; CMP: Common myeloid progenitor cells; cDC: Conventional dentritic cell; DC: Dentritic cell; EGFR: Epidermal growth factor receptor; GMP: Granulocyte- macrophage progenitors; HSC: Hematopoietic stem cells; iDC: Immature dentritic cell; JAK/STAT: Janus kinase-signal transducer and activator of transcription; LAG-3: Lymphocyte activation gene 3; LUAD: Lung adenocarcinoma; ly: Lymphatic; MAPK: Mitogen-activated protein kinase; MEP: Megakaryocyte-erythrocyte progenitors; MPP: Multipotent blood progenitors; MSC: Mesenchymal stem cell; mv: Microvascular; NFkB: Nuclear factor kappa-B; NK: Natural killer; NKT: Natural killer T; PD-1: Programmed death 1; pDC: Plasmacytoid dendritic cell; PI3K: Phosphatidylinositol 3-kinase; SCC: Squamous cell carcinoma; TCGA: The Cancer Genome Atlas; Tcm: Central memory T cell; Tgd: $\gamma\delta$T Cell; TGFβ: Transforming growth factor-β; TNFα: Tumor necrosis factor-α; Th1: T helper 1; Th2: T helper 2; VEGF: Vascular endothelial growth factor; Tregs: Regulatory T cell.

Data availability

Data are available upon reasonable request. All data relevant to this study are included in the article or online supplementary materials.

CRediT authorship contribution statement

Lishu Zhao: Writing – review & editing, Writing – original draft, Software, Methodology, Investigation, Data curation, Conceptualization. **Chen Tang:** Writing – review & editing, Writing – original draft,

Visualization, Software, Methodology, Investigation, Formal analysis. **Xuan Jin:** Writing – review & editing, Visualization, Formal analysis. **Hao Wang:** Writing – review & editing, Investigation, Data curation. **Kandi Xu:** Writing – review & editing, Project administration, Data curation. **Xinyue Liu:** Writing – review & editing, Formal analysis, Data curation. **Yujin Liu:** Writing – review & editing, Formal analysis, Data curation. **Wencheng Zhao:** Writing – review & editing, Data curation, Conceptualization. **Wengang Zhang:** Writing – review & editing, Data curation, Conceptualization. **Li Ye:** Writing – review & editing, Data curation, Conceptualization. **Zhimin Chen:** Writing – review & editing, Data curation, Conceptualization. **Qi Liu:** Writing – review & editing, Project administration, Data curation, Conceptualization. **Yayi He:** Writing – review & editing, Writing – original draft, Resources, Project administration, Funding acquisition, Data curation, Conceptualization.

Declaration of competing interest

The authors declare that they have no known competing financial interests or personal relationships that could have appeared to influence the work reported in this paper.

Funding

This study was supported in part by a grant from the National Key Research and Development Program of China (No. 2022YFF0705300); the National Natural Science Foundation of China (No. 52272281); the Shanghai Municipal Science and Technology Major Project (No. 2021SHZDZX0100); the Fundamental Research Funds for the Central Universities, Shanghai Municipal Health Commission Health Industry Clinical Research Project, Clinical Research Project of Shanghai Pulmonary Hospital (No. FKLY20010); Young Talents in Shanghai (No. 2019 QNBJ), Shanghai Shuguang Scholar, 2021 Science and Technology Think Tank Youth Talent Plan of China Association for Science and Technology, “Dream Tutor” Outstanding Young Talents Program (No. fkyq1901); and the National Key Research and Development Program of China (Nos. 2021YFF1201200 and 2021YFF1200900).

Supplementary materials

Supplementary material associated with this article can be found, in the online version, at doi:10.1016/j.pccm.2025.02.004.

References

1. Siegel RL, Miller KD, Jemal A. Cancer statistics, 2020. *CA Cancer J Clin*. 2020;70:7–30. doi:10.3322/caac.21590.
2. Xu K, Wang H, Li S, et al. Changing profile of lung cancer clinical characteristics in China: over 8-year population-based study. *Chin Med J Pulm Crit Care Med*. 2023;1:188–194. doi:10.1016/j.pccm.2023.08.006.
3. Horvath L, Thienpont B, Zhao L, Wolf D, Pircher A. Overcoming immunotherapy resistance in non-small cell lung cancer (NSCLC) – Novel approaches and future outlook. *Mol Cancer*. 2020;19:141. doi:10.1186/s12943-020-01260-z.
4. Esposito G, Palumbo G, Carillio G, et al. Immunotherapy in small cell lung cancer. *Cancers (Basel)*. 2020;12:2522. doi:10.3390/cancers12092522.
5. Huang MY, Jiang XM, Wang BL, Sun Y, Lu JJ. Combination therapy with PD-1/PD-L1 blockade in non-small cell lung cancer: strategies and mechanisms. *Pharmacol Ther*. 2020;219:107694. doi:10.1016/j.pharmthera.2020.107694.
6. Nirschl CJ, Drake CG. Molecular pathways: coexpression of immune checkpoint molecules: signaling pathways and implications for cancer immunotherapy. *Clin Cancer Res*. 2013;19:4917–4924. doi:10.1158/1078-0432.Ccr-12-1972.
7. Chen C, Liang C, Wang S, et al. Expression patterns of immune checkpoints in acute myeloid leukemia. *J Hematol Oncol*. 2020;13:28. doi:10.1186/s13045-020-00853-x.
8. Liu Y, Chen P, Wang H, et al. The landscape of immune checkpoints expression in non-small cell lung cancer: a narrative review. *Transl Lung Cancer Res*. 2021;10:1029–1038. doi:10.21037/tlcr-20-1019.
9. Sun H, Dai J, Zhao L, et al. Lymphocyte activation gene-3 is associated with programmed death-ligand 1 and programmed cell death protein 1 in small cell lung cancer. *Ann Transl Med*. 2021;9:1468. doi:10.21037/atm-21-4481.
10. He Y, Yu H, Rozeboom L, et al. LAG-3 protein expression in non-small cell lung cancer and its relationship with PD-1/PD-L1 and tumor-infiltrating lymphocytes. *J Thorac Oncol*. 2017;12:814–823. doi:10.1016/j.jtho.2017.01.019.
11. Datar I, Sanmamed MF, Wang J, et al. Expression analysis and significance of PD-1, LAG-3, and TIM-3 in human non-small cell lung cancer using spatially resolved and multiparametric single-cell analysis. *Clin Cancer Res*. 2019;25:4663–4673. doi:10.1158/1078-0432.Ccr-18-4142.
12. Zhao L, Wang H, Xu K, Liu X, He Y. Update on lymphocyte-activation gene 3 (LAG-3) in cancers: from biological properties to clinical applications. *Chin Med J (Engl)*. 2022;135:1203–1212. doi:10.1097/cm9.0000000000001981.
13. Lecocq Q, Keyaerts M, Devoogdt N, Breckpot K. The next-generation immune checkpoint LAG-3 and its therapeutic potential in oncology: third time’s a charm. *Int J Mol Sci*. 2020;22:75. doi:10.3390/ijms22010075.
14. Felip E, Doger B, Majem M, et al. Initial results from a phase II study (TACTI-002) in metastatic non-small cell lung or head and neck carcinoma patients receiving eftilagimod alpha (soluble LAG-3 protein) and pembrolizumab. *J Clin Oncol*. 2020;38:3100. doi:10.1200/JCO.2020.38.15_suppl.3100.
15. Lipson EJ, Tawbi HA, Schadendorf D, et al. Relatlimab (RELA) plus nivolumab (NIVO) versus NIVO in first-line advanced melanoma: primary phase III results from RELATIVITY-047 (CA224-047). *J Clin Oncol*. 2021;39:9503. doi:10.1200/JCO.2021.39.15_suppl.9503.
16. He Y, Guo H, Diao L, et al. Prediction of driver gene matching in lung cancer NOG/PDX models based on artificial intelligence. *Engineering*. 2022;15:102–114. doi:10.1016/j.eng.2021.06.017.
17. Wu F, Fan J, He Y, et al. Single-cell profiling of tumor heterogeneity and the microenvironment in advanced non-small cell lung cancer. *Nat Commun*. 2021;12:2540. doi:10.1038/s41467-021-22801-0.
18. He Y, Liu X, Wang H, et al. Mechanisms of progression and heterogeneity in multiple nodules of lung adenocarcinoma. *Small Methods*. 2021;5:e2100082. doi:10.1002/smtd.202100082.
19. Sangro B, Melero I, Wadhawan S, et al. Association of inflammatory biomarkers with clinical outcomes in nivolumab-treated patients with advanced hepatocellular carcinoma. *J Hepatol*. 2020;73:1460–1469. doi:10.1016/j.jhep.2020.07.026.
20. Lei M, Siemers NO, Pandya D, et al. Analyses of PD-L1 and inflammatory gene expression association with efficacy of nivolumab ± ipilimumab in gastric cancer/gastroesophageal junction cancer. *Clin Cancer Res*. 2021;27:3926–3935. doi:10.1158/1078-0432.Ccr-20-2790.
21. Tawbi HA, Schadendorf D, Lipson EJ, et al. Relatlimab and nivolumab versus nivolumab in untreated advanced melanoma. *N Engl J Med*. 2022;386:24–34. doi:10.1056/NEJMoa2109970.
22. Fang W, Jin H, Zhou H, et al. Intratumoral heterogeneity as a predictive biomarker in anti-PD-(L)1 therapies for non-small cell lung cancer. *Mol Cancer*. 2021;20:37. doi:10.1186/s12943-021-01331-9.
23. Wang J, Sanmamed MF, Datar I, et al. Fibrinogen-like protein 1 is a major immune inhibitory ligand of LAG-3. *Cell*. 2019;176:334–347.e12. doi:10.1016/j.cell.2018.11.010.
24. Kouo T, Huang L, Pucsek AB, et al. Galectin-3 shapes antitumor immune responses by suppressing CD8+ T cells via LAG-3 and inhibiting expansion of plasmacytoid dendritic cells. *Cancer Immunol Res*. 2015;3:412–423. doi:10.1158/2326-6066.Cir-14-0150.
25. Xu F, Liu J, Liu D, et al. LSECtin expressed on melanoma cells promotes tumor progression by inhibiting antitumor T-cell responses. *Cancer Res*. 2014;74:3418–3428. doi:10.1158/0008-5472.Can-13-2690.
26. Grosso JF, Kelleher CC, Harris TJ, et al. LAG-3 regulates CD8+ T cell accumulation and effector function in murine self- and tumor-tolerance systems. *J Clin Invest*. 2007;117:3383–3392. doi:10.1172/jci31184.
27. Hannier S, Triebel F. The MHC class II ligand lymphocyte activation gene-3 is co-distributed with CD8 and CD3–TCR molecules after their engagement by mAb or peptide–MHC class I complexes. *Int Immunol*. 1999;11:1745–1752. doi:10.1093/intimm/11.11.1745.
28. Wang M, Du Q, Jin J, Wei Y, Lu Y, Li Q. LAG3 and its emerging role in cancer immunotherapy. *Clin Transl Med*. 2021;11:e365. doi:10.1002/ctm2.365.
29. de Visser KE, Joyce JA. The evolving tumor microenvironment: from cancer initiation to metastatic outgrowth. *Cancer Cell*. 2023;41:374–403. doi:10.1016/j.ccell.2023.02.016.
30. Fukumura D, Kloepper J, Amoozgar Z, Duda DG, Jain RK. Enhancing cancer immunotherapy using antiangiogenics: opportunities and challenges. *Nat Rev Clin Oncol*. 2018;15:325–340. doi:10.1038/nrclinonc.2018.29.
31. Le X, Nilsson M, Goldman J, et al. Dual EGFR-VEGF pathway inhibition: a promising strategy for patients with EGFR-mutant NSCLC. *J Thorac Oncol*. 2021;16:205–215. doi:10.1016/j.jtho.2020.10.006.
32. Finn RS, Kudo M, Cheng AL, et al. Pharmacodynamic biomarkers predictive of survival benefit with lenvatinib in unresectable hepatocellular carcinoma: from the phase III REFLECT study. *Clin Cancer Res*. 2021;27:4848–4858. doi:10.1158/1078-0432.Ccr-20-4219.
33. Mollinedo F. Neutrophil degranulation, plasticity, and cancer metastasis. *Trends Immunol*. 2019;40:228–242. doi:10.1016/j.it.2019.01.006.
34. Li K, Tandurella JA, Gai J, et al. Multi-omic analyses of changes in the tumor microenvironment of pancreatic adenocarcinoma following neoadjuvant treatment with anti-PD-1 therapy. *Cancer Cell*. 2022;40:1374–1391.e1377. doi:10.1016/j.ccell.2022.10.001.
35. Rosales C. Neutrophils at the crossroads of innate and adaptive immunity. *J Leukoc Biol*. 2020;108:377–396. doi:10.1002/jlb.4mir0220-574rr.
36. Kaisar-Iluz N, Arpinati L, Shaul ME, et al. The bilateral interplay between cancer immunotherapies and neutrophils’ phenotypes and sub-populations. *Cells*. 2022;11:783. doi:10.3390/cells11050783.
37. Babačić H, Lehtiö J, Pico de Coaña Y, Pernemalm M, Eriksson H. In-depth plasma proteomics reveals increase in circulating PD-1 during anti-PD-1 immunotherapy in patients with metastatic cutaneous melanoma. *J Immunother Cancer*. 2020;8:e000204. doi:10.1136/jitc-2019-000204.